

Microphysical Pathways Active within Thunderstorms and Their Sensitivity to CCN Concentration and Wind Shear

Andrew Ian Barrett¹ and Corinna Hoose²

¹Karlsruhe Institute for Technology

²Karlsruhe Institute of Technology

November 23, 2022

Abstract

The impact of cloud condensation nuclei (CCN) concentration on microphysical processes within thunderstorms and the resulting surface precipitation is not fully understood yet. In this work, an analysis of the microphysical pathways occurring in these clouds is proposed to systematically investigate and understand these sensitivities. Thunderstorms were simulated using convection-permitting (1 km horizontal grid spacing) idealised simulations with the ICON model, which included a 2-moment microphysics parameterization. CCN concentrations were increased from 100 to 3200 CCN/cm³, in five different wind shear environments ranging from 18 to 50 m/s. Large and systematic decreases of surface precipitation (up to 35%) and hail (up to 90%) were found as CCN was increased. Wind shear changes the details, but not the sign, of the sensitivity to CCN. The microphysical process rates were tracked throughout each simulation, closing the mass budget for each hydrometeor class, and collected together into “microphysical pathways”, which quantify the different growth processes leading to surface precipitation. Almost all surface precipitation occurred through the mixed-phase pathway, where graupel and hail grow by riming and later melt as they fall to the surface. The mixed-phase pathway is sensitive to CCN concentration changes as a result of changes to the riming rate, which were systematically evaluated. Supercooled water content was almost insensitive to increasing CCN concentration, but decreased cloud drop size led to a large reduction in the riming efficiency (from 0.79 to 0.24) between supercooled cloud drops and graupel or hail, resulting in less surface precipitation.

1 **Microphysical Pathways Active within Thunderstorms**
2 **and Their Sensitivity to CCN Concentration and Wind**
3 **Shear**

4 **Andrew I. Barrett¹, Corinna Hoose¹**

5 ¹Institute for Meteorology and Climate Research, Karlsruhe Institute of Technology, Karlsruhe, Germany

6 **Key Points:**

- 7 • Microphysical pathways are constructed by tracking microphysical processes rates
8 and closing the hydrometeor mass budget.
- 9 • More CCN lead to less surface precipitation and hail, due to smaller cloud drop
10 sizes and reduced riming collection efficiency.
- 11 • Simulations with constant riming collection efficiency reveal two different hail for-
12 mation pathways.

Corresponding author: Andrew I. Barrett, andrew.barrett@kit.edu

Corresponding author: Corinna Hoose, corinna.hoose@kit.edu

Abstract

The impact of cloud condensation nuclei (CCN) concentration on microphysical processes within thunderstorms and the resulting surface precipitation is not fully understood yet. In this work, an analysis of the microphysical pathways occurring in these clouds is proposed to systematically investigate and understand these sensitivities. Thunderstorms were simulated using convection-permitting (1 km horizontal grid spacing) idealised simulations with the ICON model, which included a 2-moment microphysics parameterization. CCN concentrations were increased from 100 to 3200 CCN/cm³, in five different wind shear environments ranging from 18 to 50 m/s. Large and systematic decreases of surface precipitation (up to 35%) and hail (up to 90%) were found as CCN was increased. Wind shear changes the details, but not the sign, of the sensitivity to CCN. The microphysical process rates were tracked throughout each simulation, closing the mass budget for each hydrometeor class, and collected together into “microphysical pathways”, which quantify the different growth processes leading to surface precipitation. Almost all surface precipitation occurred through the mixed-phase pathway, where graupel and hail grow by riming and later melt as they fall to the surface. The mixed-phase pathway is sensitive to CCN concentration changes as a result of changes to the riming rate, which were systematically evaluated. Supercooled water content was almost insensitive to increasing CCN concentration, but decreased cloud drop size led to a large reduction in the riming efficiency (from 0.79 to 0.24) between supercooled cloud drops and graupel or hail, resulting in less surface precipitation.

1 Introduction

Thunderstorms produce numerous weather hazards including lightning, strong winds and extreme precipitation. Precipitation rates above 100 mm/hr and hail larger than 5 cm is frequently reported from the most intense thunderstorms. The rain drops, hail stones and other precipitation hydrometeors are formed within thunderstorms as the result of various microphysical processes (such as growth by condensation, collisions with other hydrometeors, freezing and melting, among others). A chain of several microphysical processes is usually responsible for the formation of precipitating hydrometeors; several chains exist within convective storms although not all are necessarily active in any particular storm or at a particular time. We refer to these chains of microphysical processes as “microphysical pathways” throughout this paper.

45 The amount and type of surface precipitation produced within thunderstorms is
46 sensitive to environmental conditions. Larger and more organised thunderstorms are more
47 likely to form when the wind shear (often defined as vector difference between winds at
48 0 and 6 km) increases. Increased wind shear can increase the width of the storm updraft
49 [Warren *et al.*, 2017; Marion and Trapp, 2019], the storm lifetime and therefore the over-
50 all precipitation total.

51 Similarly, the aerosol concentration in the atmosphere also affects the precipita-
52 tion process by modifying the number and size of hydrometeors within clouds. The aerosols,
53 by virtue of their ability to act as cloud condensation nuclei (CCN) or ice nucleating par-
54 ticles (INP), affect the cloud properties and therefore microphysical processes. Increased
55 CCN concentrations lead to more numerous but smaller cloud drops at cloud base. In-
56 creased INP concentrations lead to freezing at higher temperatures or faster glaciation.
57 However, the overall impact of aerosols on convective precipitation remains uncertain
58 [Tao *et al.*, 2012]. Neither observational nor modelling studies are currently able to pro-
59 vide a clear picture. Variability of CCN in observational studies cannot be fully sepa-
60 rated from meteorological variability, which makes it impossible to attribute differences
61 in cloud or precipitation quantities to changing CCN alone [Stevens and Feingold, 2009].
62 Modelling studies allow for meteorological and CCN variables to be varied independently;
63 however, results from different models, environments, days and timescales give almost
64 every possible sensitivity to CCN concentration [Khain *et al.*, 2008].

65 Recent increases in modelling and computational abilities have enabled CCN ef-
66 fects on convective clouds to be simulated at high resolution. The sensitivity of hail to
67 increasing CCN concentration is particularly uncertain. Multiple studies show that hail
68 amount can increase [Khain *et al.*, 2011a; Loftus and Cotton, 2014; Khain *et al.*, 2015;
69 Chen *et al.*, 2019], or decrease [Noppel *et al.*, 2010; Morrison, 2012; Wellmann *et al.*, 2018;
70 Barrett *et al.*, 2019]. Some of these studies also report non-systematic sensitivities [e.g.
71 Noppel *et al.*, 2010] with increasing CCN concentration. Other studies show that the sen-
72 sitivity depends on other factors. For example, Carrió *et al.* [2014] found a dependence
73 on cloud base height, while Morrison [2012] found that the inclusion of an additional hail
74 hydrometeor class changed the sign of the sensitivity, as did changing the assumed fall
75 velocity of hail to that of snow. These studies used a variety of 2D or 3D simulations,
76 different microphysical parameterizations of various complexity (2-moment, 3-moment,
77 bin microphysics) and analysed simulations of either idealised or real cases. These dif-

78 differences in CCN sensitivity likely result from the different assumptions within the mi-
79 crophysical parameterizations; however, we still lack convincing explanations for these
80 diverse results.

81 One way to improve our understanding of these different sensitivities is to better
82 understand the physical mechanisms through which precipitation is formed and how these
83 mechanisms are affected by CCN concentration in different modelling setups. By under-
84 standing how each of the microphysical pathways is represented in each model and how
85 sensitive they each are to CCN concentration in different situations could help us to dis-
86 entangle their different sensitivities.

87 In this work, we analyse the sensitivity of surface precipitation to CCN concentra-
88 tion in idealised simulations of thunderstorms using the ICON model. We explore the
89 potential that a deep analysis of the microphysical pathways can offer. Furthermore, we
90 determine whether the sensitivity to CCN and important microphysical pathways remains
91 constant as the wind shear is increased.

92 Details about the model, model setup and selected microphysical parameterizations
93 are given in section 2. Using the microphysical pathways outlined and quantified in sec-
94 tion 2.3, precipitation and hail statistics from the simulation are analysed in section 3.
95 The causes of the sensitivities are discussed in section 4. Section 5 contains discussion
96 of the relevance of the work and conclusions are drawn in section 6.

97 **2 Model and methods**

98 **2.1 Model experimental setup**

99 A short, idealized simulation with the ICON model, version 2.6.2.2, is used for each
100 setup. The model is initialized with the temperature and humidity profiles of *Weisman*
101 *and Klemp* [1982] and westerly winds increasing with height from zero at the surface up
102 to 6 km altitude. All fields are horizontally-homogeneous at initialization. Convection
103 is initiated by the release of a 3 K warm bubble in the first timestep. The first two hours
104 are simulated, during which dynamical feedbacks to the updraft are limited and are there-
105 fore comparable for all CCN concentrations. The idealised simulation is justified as we
106 are interested mainly in in-cloud processes rather than the specifics of convective initi-
107 ation.

108 To study the sensitivity of precipitation and hail formation to CCN concentration
 109 and wind shear, 20 simulations are run. Four different CCN concentrations are chosen:
 110 100, 500, 1700, 3200 CCN/cm³; CCN are uniformly distributed in the horizontal, and
 111 decrease exponentially above 4 km with a scale height of 4 km. The horizontal winds are
 112 purely westerly, increasing linearly from zero at the surface to u_{max} at and above 6 km
 113 altitude; u_{max} values of 18, 25, 32, 42, 50 m/s are used. Each simulation is 2 hours du-
 114 ration, and the sensitivities are evaluated at the end of this 2-hour period. Abbreviations
 115 of the form CCN100 are used to refer to all simulations with 100 CCN/cm³; similarly
 116 WS18 refers to all simulations with 18 m/s wind shear. Specific simulations are referred
 117 to by combining these (for example WS18+CCN100).

118 The model setup used for this study is summarized in Table 1. Specific details rel-
 119 evant for this study are explained in the following subsections.

121 **2.2 Microphysics parameterization**

122 In this study, the 2-moment bulk microphysics scheme of *Seifert and Beheng* [2006a,b],
 123 with the additional hail category [*Blahak*, 2008] is used. The main processes important
 124 for discussions within this paper are described here. For a more complete description of
 125 the parameterization scheme, readers are referred to the original papers.

126 **Condensation**

127 Condensation within ICON is performed before the call to the parameterized mi-
 128 crophysics. This is performed through saturation adjustment, where any supersatura-
 129 tion produced through the model dynamics is removed and an appropriate amount of
 130 cloud water and latent heating is produced such that the grid box achieves 100% rela-
 131 tive humidity. Similarly, cloud water is evaporated in sub-saturated environments. The
 132 use of saturation adjustment can potentially limit aerosol-convection interactions [*Lebo*
 133 *et al.*, 2012]; however, the aim of this study is to determine how microphysical pathways
 134 are changed after cloud water has been formed which should be largely unaffected.

135 **CCN activation**

136 The cloud condensation nuclei (CCN) activation uses the lookup tables by *Segal*
 137 *and Khain* [2006], which determine the number of activated cloud droplets based on ver-
 138 tical velocity. Activation of CCN occurs only where supersaturation with respect to liq-
 139 uid exists and grid-scale vertical velocity is positive (upward). However, it is the verti-

Table 1. Details of the ICON model setup used for this study.

Parameter	Value / reference
Model grid	
Horizontal Resolution	1 km
Vertical Levels	100
Domain	300×100 km torus (double-periodic boundaries)
Model integration	
Timestep	3 seconds
Duration	2 hours
Environmental setup	
Thermodynamic profile	unstable [<i>Weisman and Klemp, 1982</i>]
Convection initiation	warm bubble (+3 K, 15 km radius)
Wind profile	westerly winds; linear increase to maximum speed (18–50 m/s), at and above 6 km
CCN concentration	100–3200 CCN/cm ³ , horizontally uniform, constant up to 4 km, exponential decrease above [<i>Noppel et al., 2010</i>]
Physics parameterizations	
Cloud microphysics	two-moment, six-category scheme [<i>Seifert and Beheng, 2006a; Blahak, 2008</i>]
CCN activation	[<i>Segal and Khain, 2006</i>]
Radiation	none
Ice nucleation	volume-dependent rain drop freezing [<i>Bigg, 1953</i>], immersion freezing of cloud droplets and deposition nucleation [<i>Phillips et al., 2008</i>]

cal velocity, rather than supersaturation, which is used to determine the number of CCN
 that are activated. Activation of CCN can occur both at cloud base, and within the cloud
 at grid-boxes where supersaturation exists at the beginning of the cloud microphysics
 calculations. CCN concentrations used in this paper are 100, 500, 1700, 3200 CCN/cm³.
 These CCN concentrations are constant in the lowest 4 km but decrease exponentially
 with height above 4 km, with a scale height of 2 km.

146 **Autoconversion and accretion** (converting cloud water to rain water)

147 The autoconversion of cloud drops to rain, and the accretion of cloud drops by falling
 148 rains drops are parameterized following *Seifert and Beheng* [2001]. The autoconversion
 149 rate approximately scales with $L_c^2 x_c^2$, where L_c is the cloud water content in kg/m³ and
 150 x_c is the mean mass of cloud drops. The full equations are given by *Seifert and Beheng*
 151 [2006a, eqns. 4-6.] Accretion rate approximately scales with $L_c L_r$, where L_r is the rain
 152 water content in kg/m³. The full equations are given by *Seifert and Beheng* [2006a, eqns.
 153 7-8.].

154 **Rain freezing**

155 The freezing of rain drops is parameterized in two stages. First the freezing rate
 156 of rain drops is determined from the parameterization of *Bigg* [1953], depending on tem-
 157 perature and rain drop mean size. Second, the fraction of these frozen drops becoming
 158 snow, graupel or hail is determined by the size of rain drops within the gridbox. Rain
 159 drops with diameters below 500 μm become ice; between 500 and 1250 μm become grau-
 160 pel and rain drops with diameter larger than 1250 μm become hail. Heterogeneous and
 161 homogeneous freezing of cloud droplets as well as heterogeneous ice nucleation from the
 162 vapour phase are not relevant for the microphysical pathways leading to surface precip-
 163 itation and are therefore not discussed here.

164 **Graupel formation**

165 Graupel is either formed directly from rain freezing (see above) or from riming on
 166 to ice or snow. When the riming rate within a grid box exceeds the rate of growth by
 167 vapor deposition, the ice (or snow) becomes graupel. All mass and number at this grid
 168 point is moved from the ice (or snow) category to the graupel category.

169 **Hail formation**

170 Hail is either formed directly from rain freezing (see above) or when riming onto
 171 graupel particles leads to “wet growth”; where latent heating of freezing increases the

172 hydrometeor surface temperature above 0°C. Threshold sizes are determined in the model
 173 using lookup tables, based on temperature and liquid water content. The mass and num-
 174 ber of graupel stones experiencing wet growth are moved to the hail category.

175 **Riming**

176 Riming can occur when a frozen hydrometeor collides with a liquid hydrometeor.
 177 The number of collisions is parameterized taking into account the full size distribution
 178 of both frozen and liquid hydrometeors and their respective fall velocities. Each colli-
 179 sion type has an associated collection efficiency, based on particle types and mean sizes
 180 *Seifert and Beheng* [2006a]. After all collisions are calculated, the mass and number of
 181 liquid hydrometeors which are collected are moved to the frozen category of the collec-
 182 tor. In some cases, riming leads to a change of the frozen hydrometeor classification (see
 183 graupel formation and hail formation above).

184 **2.3 Possible pathways**

185 To simplify the numerous interactions of microphysical processes inside the model,
 186 we attempt to reduce the complexity by grouping the processes into a number of pos-
 187 sible microphysical pathways. Each pathway represents a possible path for hydromete-
 188 ors to grow, freeze, melt and evaporate on their way to reaching the surface or, alterna-
 189 tively, remaining suspended in the atmosphere or returning to the vapor phase. The rel-
 190 ative importance of each pathway is quantified for our simulations in section 3.3. In the
 191 most simplified form, there are essentially four possible pathways that hydrometeors can
 192 follow:

- 193 1. **warm-rain pathway:** Cloud water is produced through condensation. Cloud droplets
 194 grow through collision and coalescence, forming rain (“autoconversion” in model
 195 parameterizations). Rain droplets form before freezing occurs. Rain droplets fall
 196 through the cloud, collecting other cloud and rain drops (“accretion”) as they fall.
 197 Rain drop fall from the cloud, begin to evaporate and may reach the surface.
- 198 2. **mixed-phase pathway :** Convection reaches heights where the air is cold enough
 199 for freezing to begin (at least -4°C). Some supercooled water freezes. These frozen
 200 drops collide with and collect (“riming”) supercooled liquid drops (either cloud
 201 or rain), forming graupel and later hail. Graupel and hail fall to the melting level
 202 while continuing to collect mass by riming. Melting below the melting level be-

gins to form rain; the unmelted parts of the frozen particles fall to the surface, as do the rain drops formed by melting (subject to evaporation).

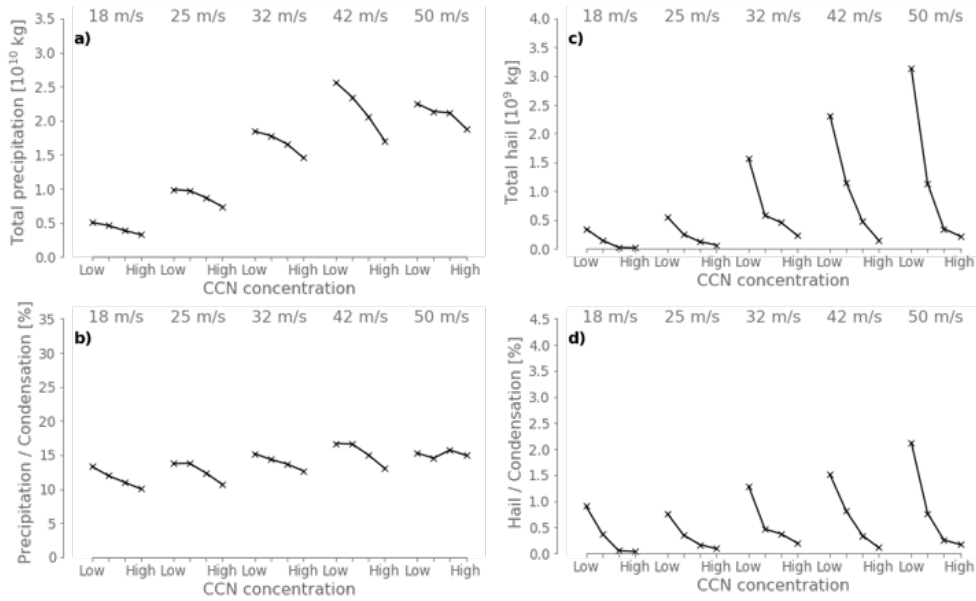
3. **ice-phase pathway** : Convection reaches heights where freezing occurs. No significant riming occurs, either because the freezing is so efficient that all water freezes or the liquid water content is sufficiently low. Vapor deposition allows the ice particles to grow and the liquid evaporates (Wegener-Bergeron-Findeisen process). Frozen particles (ice or snow) grow by colliding with and collecting other frozen particles (“aggregation”) and/or by vapor deposition. Ice and snow particles fall to the melting level. Particle melting begins to form rain, or the frozen particles fall to the surface.
4. **non-precipitating pathway**: particles follow pathway 2 or 3; however, the growth is sufficiently slow that the particles do not achieve fall velocities that (notably) exceeds the air vertical velocity and therefore neither grow nor fall. These hydrometeors remain lofted in the atmosphere (for example in a convective anvil) and eventually their mass returns to the vapor phase as evaporation or sublimation occurs.

3 Results

3.1 Precipitation and hail totals

The total precipitation and hail mass reaching the surface are sensitive to both CCN concentration and wind shear (Figure 1). Precipitation systematically increases with increasing wind shear and hail generally increases with wind shear (in 82% of simulation pairs). Precipitation and hail both systematically decrease with increasing CCN concentration. The high-shear, low-CCN (WS42+CCN100) simulation produces the most precipitation (domain average: 0.931 mm) whereas the low-shear, high-CCN (WS18+CCN3200) simulation produces the least (0.068 mm). The explanation and reasons behind these differences are detailed in the following two sections.

The total surface precipitation increases steadily with time through the simulation, whereas the hail formation appears to cycle between active and less active periods, especially when wind shear is 32 m/s or above (Figure 2). Importantly, the ordering of simulations from low to high surface precipitation or surface hail is almost fully consistent throughout the 2-hour simulation period (Figure 2), meaning that the results are not dependent on this specific evaluation time. Similarly, the ordering of simulations based on precipitation and hail flux at a certain distance below cloud base is consistent (not shown),



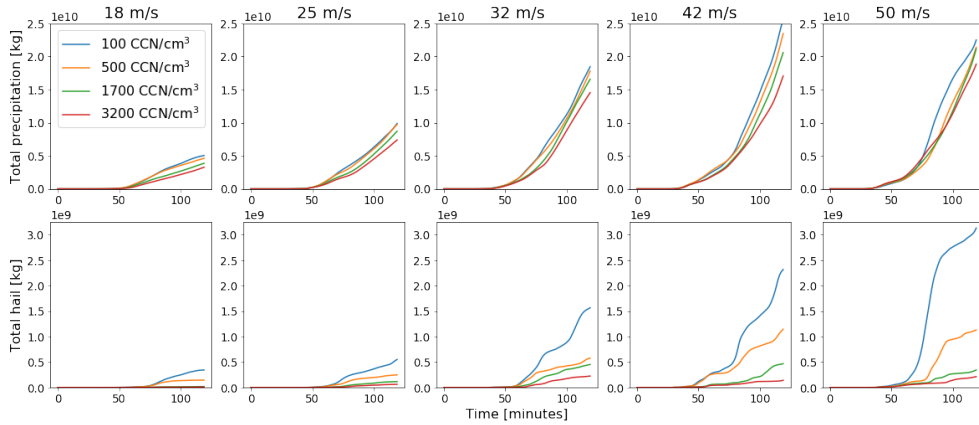
220 **Figure 1.** Accumulated precipitation (a) and surface hail fall (b) in each simulation. Wind
 221 shear is given above the plots, while the four symbols for each wind shear represent the four CCN
 222 cases. The lower two plots show the precipitation efficiency for rain (b) and hail (d), by normalis-
 223 ing the quantities in the top row by the total condensation occurring within the simulation.

241 indicating that analysis of these simulations after 2 hours and at the surface is robust
 242 and representative of the simulations on the whole.

243 3.2 2D structure of convective cells

258 The vertical and horizontal structure of hydrometeors within the convective cells,
 259 and the process leading to addition or removal of mass from each hydrometeor category
 260 were created through compositing. An example for the WS18+CCN100 simulation (Fig-
 261 ure 3) highlights the major source and sink regions of hydrometeor mass for the differ-
 262 ent microphysical pathways.

263 Rain is produced within the updraft core (Figure 3a), through collision and coa-
 264 lence of cloud droplets (model processes: autoconversion and accretion). Between 6–
 265 9 km altitude these rain drops begin to freeze (rain freezing) and then are collected by
 266 frozen hydrometeors (riming). This freezing and riming means that no rain mass is trans-
 267 ported above 9 km altitude and happens before the rain drops leave the updraft and fall
 268 toward the ground. The importance of the freezing and riming processes mean the warm-

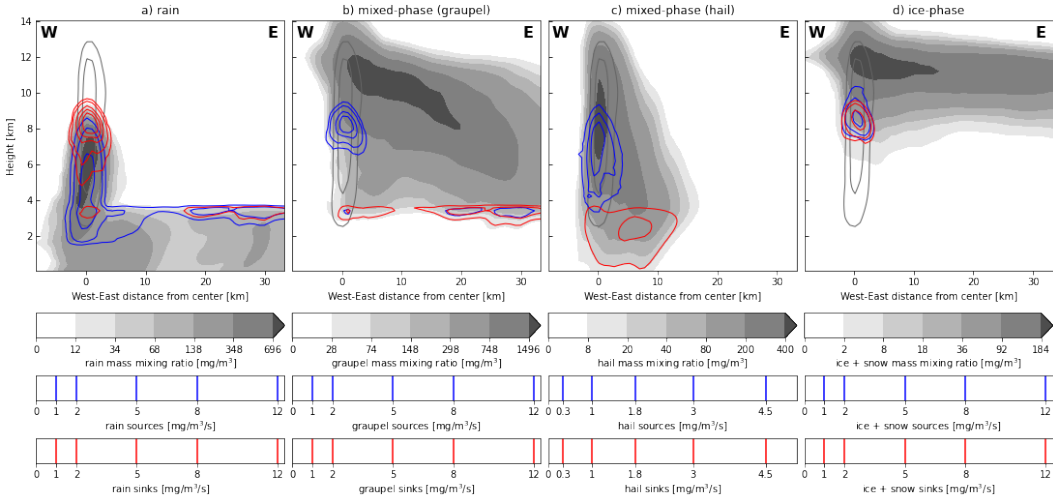


232 **Figure 2.** Timeseries of domain-integrated accumulated precipitation (top row) and total hail
 233 fall (bottom row).

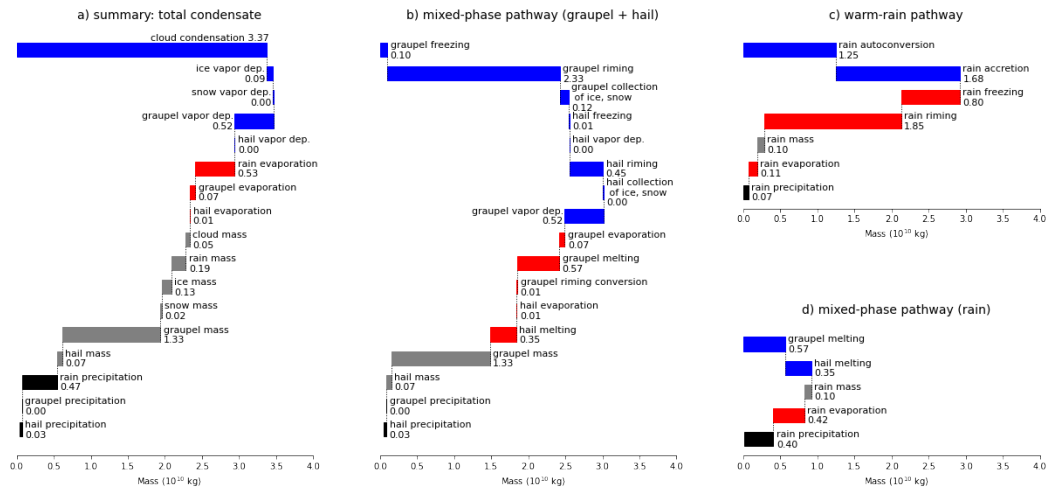
269 rain pathway is almost inactive, but that the precipitation is produced via the mixed-
 270 phase pathway. Rain mass is formed in the mixed-phase pathway through melting of grau-
 271 pel and hail, starting just below 4 km altitude.

272 Graupel is initially formed by freezing of rain drops (Figure 3b), of through con-
 273 version of ice and snow to graupel as they begin to rime. However, most of the mass is
 274 formed by riming within the updraft core above 7 km and much of the mass remains sus-
 275 pended in the atmosphere. Graupel which is able to fall to 4 km, quickly melts in a nar-
 276 row melting layer.

277 Hail (Figure 3c) forms either when large rain drops freeze or from a reclassifica-
 278 tion of graupel when the “wet-growth” regime is reached. As for graupel, hail mass mainly
 279 comes from riming, but the location is different from riming onto graupel. Due to slight
 280 rotation within the updraft, hail embryos are produced by freezing large raindrops on
 281 the eastern side of the updraft (where the largest raindrops are). These embryos are then
 282 transported from east to west across the updraft, with most of the riming occurring on
 283 the western side of the updraft (where the hail embryos have grown larger and the rain
 284 mass is most concentrated). Hail riming occurs either at the same altitude and lower than
 285 graupel riming. The largest hail stones fall more quickly than graupel and can reach the
 286 melting level on the north side of the updraft core. Smaller hail stones are continually
 287 lifted by the updraft above the region where riming is possible, limiting their growth.
 288 These small hail stones fall to the ground more quickly than graupel particles and there-



244 **Figure 3.** West-East cross-sections through the convective cell in the WS18+CCN100 simu-
245 lation showing the relative locations of hydrometeor mass (grey shading), sources of mass (blue
246 contours) and sinks of mass (red contours) for four different hydrometeor categories a) rain, b)
247 graupel, c) hail and d) ice and snow combined. Composites are built using values at 5-minute
248 intervals between 45 and 90 minutes simulation time, centred on the cell maximum updraft loca-
249 tion at 5 km altitude. Black contour lines are updraft velocities of 10 and 20 m/s. and Contour
250 line intervals for the sources and sinks are given one the scales below the plots.



251 **Figure 4.** Waterfall plots showing process rates which contribute to the different microphys-
 252 ical pathways. Values are for the WS18+CCN100 simulation and show whole domain integrals
 253 (time and height) for the 2-hour simulation period. Blue represents sources of hydrometeor mass
 254 in each pathway and red represents sinks of mass, gray represents mass of hydrometeors in the
 255 atmosphere and black represents surface precipitation. Note: graupel vapor deposition is shown
 256 as a source, but the net process rate is negative indicating that sublimation is more important
 257 than vapor deposition.

289 fore remain much closer to the updraft core than graupel. A broad and deep region of
290 hail melting is present below the melting level, extending to the ground. Some of the largest
291 hail stones are able to reach the surface without fully melting.

292 Ice and snow are produced through freezing of cloud and rain drops within the up-
293 draft at 8–9 km altitude (Figure 3d). Many of these particles are quickly involved in rim-
294 ing and become graupel, hence the co-located source and sink regions. Ice and snow par-
295 ticles which do not become graupel remain small and suspended in the atmosphere above
296 8 km, moving into the anvil region of the cell and being advected downwind. Ice and snow
297 do not fall to the melting level and are therefore not involved in surface precipitation for-
298 mation in this simulation.

299 Simulations with increased wind shear (not shown) produce more tilted and wider
300 updrafts. This allows rain drops to grow via collision and coalescence for a longer time
301 before either reaching the freezing temperatures or moving out of the updraft region.

302 In simulations with increased CCN concentration (not shown), the collision and
303 coalescence process occurs more slowly. Therefore, the large rain drops needed for freez-
304 ing are produced later and at higher altitudes. Consequently, less freezing and riming
305 occurs within an air parcel rising through the updraft, allowing more freezing to ice and
306 snow when homogeneous freezing begins at around -38°C . and more ice and snow re-
307 mains suspended in the atmosphere through the simulation.

308 The microphysical pathways, and the sensitivity to both CCN and wind shear, are
309 evaluated in more detail in the following section.

310 **3.3 Microphysical pathways in model simulations**

311 The importance of each microphysical pathway is calculated using high time-resolution
312 model output of hydrometeor contents and microphysical process rates. This allows us
313 to almost fully close the hydrometeor mass budget for each hydrometeor class individ-
314 ually (not shown). Process rates are combined following the possible microphysical path-
315 ways (Figure 4) and we are again able to close the mass budget overall (Figure 4a) and
316 for individual pathways (Figure 4b-d). This is shown and discussed exemplarily for the
317 WS18+CCN100 case. In this simulation, hydrometeor mass is formed mainly through
318 condensation (97%, Figure 4a), with a small additional contribution from vapor depo-

319 sition onto ice (3%). Around 15% of mass is lost via sublimation of graupel (negative
 320 vapor deposition), and another 15% from evaporation below the melting level. 0.50×10^{10} kg
 321 fell to the surface as precipitation leaving 1.29×10^{10} kg suspended in the atmosphere,
 322 mostly as graupel. This equates to a precipitation efficiency (precipitation/condensation)
 323 of 14.5% (0.50×10^{10} kg/ 3.46×10^{10} kg) in this two-hour period.

324 The microphysical pathway analysis allows to attribute the surface precipitation
 325 to either warm- or mixed-phase pathways; the ice-phase does not contribute to surface
 326 precipitation in these simulations. The mixed-phase pathway produces at least 86% of
 327 the surface precipitation (0.03×10^{10} kg hail (Figure 4b) + 0.40×10^{10} kg rain from melted
 328 graupel and hail (Figure 4d), from 0.50×10^{10} kg total precipitation). This relative con-
 329 tribution from the mixed-phase pathway is likely an underestimate, as discussed below,
 330 and therefore the warm-rain pathway (Figure 4c) barely contributes at all to surface pre-
 331 cipitation. Rain water mass produced by autoconversion and accretion of cloud water
 332 is almost completely removed by freezing and riming before it can fall out of the updraft.

333 In contrast, rain formed through melting of graupel and hail produces almost all
 334 of the surface precipitation (Figure 4d). Almost half of all rain water from melting evap-
 335 orates before reaching the ground. An equivalent amount reaches the ground as rain, with
 336 roughly 10% still falling from the cloud at the end of the simulation. More than 90% of
 337 the graupel and hail mass is produced by riming (Figure 4b), with small contributions
 338 from the freezing of rain drops and the formation of graupel embryos, which originally
 339 grew as ice or snow. Around half of the graupel mass produced during the simulation
 340 remains suspended in the atmosphere at the end, whereas the remaining more than 50%
 341 of the graupel and hail mass melts to become rain (Figure 4b and d). Of the 0.45×10^{10} kg
 342 hail mass produced during the simulation, 0.03×10^{10} kg reaches the surface while still
 343 solid, 0.07×10^{10} kg is still falling, 0.35×10^{10} kg melts to rain and 0.01×10^{10} kg evap-
 344 orates (Figure 4b).

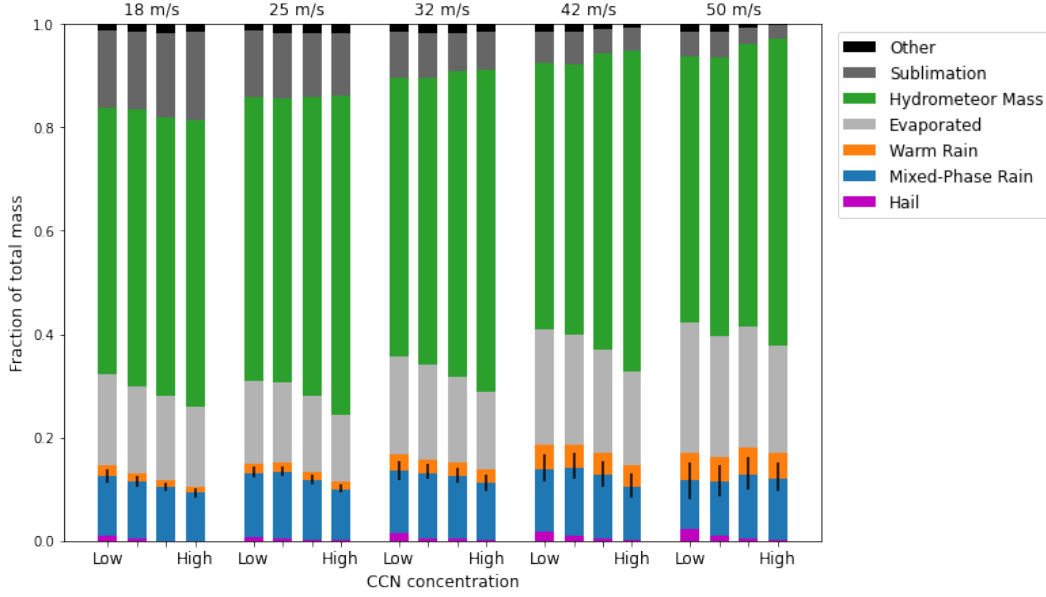
345 Analysing the microphysical pathways for all simulations shows that the largest con-
 346 tribution to surface precipitation always comes from the mixed-phase pathway (Figure 5).
 347 The mixed-phase contribution increases slightly as CCN concentration is increased. As
 348 wind shear is increased the precipitation fraction from the mixed-phase pathway decreases
 349 and becomes more uncertain. It is even possible that all surface precipitation comes from

350 the mixed-phase pathway in all simulations. The uncertainty related to this contribu-
 351 tion are discussed in the following.

352 From the analysis of simulation WS18+CCN100 we conclude that at least 86% of
 353 surface precipitation results from the formation (and later melting) of frozen hydrom-
 354 eteors (mainly graupel and hail). However, there is some ambiguity about how to allo-
 355 cate the rain mass in the atmosphere, rain evaporation and surface precipitation among
 356 the warm and mixed-phase pathways. We allocate them as follows. Rain mass above the
 357 melting level is warm rain (although it might later freeze or rime, and therefore contribute
 358 to the mixed-phase pathway). Rain mass below the melting level, total evaporation and
 359 surface precipitation are allocated to both warm and mixed-phase pathways such that
 360 the ratio of these 3 values is the same for each pathway. This assumes that evaporation
 361 of warm rain and mixed-phase rain is equal. This assumption is poor. Melted graupel
 362 and hail stones produce larger rain hydrometeors than those formed through warm rain
 363 processes. Therefore warm rain would evaporate more quickly than mixed-phase rain,
 364 meaning that the 86% estimate from the mixed-phase pathway would be an underesti-
 365 mate. To quantify these uncertainties, the separation was again performed with
 366 mass:precipitation:evaporation ratios of 1:1:5 (warm rain evaporates faster) and 5:5:1 (warm
 367 rain evaporates slower). These values are shown by the black error bars in Figure 5. For
 368 all cases, the mixed-phase pathway is more important than the warm rain pathway. The
 369 relative importance of the warm rain pathway increases with increasing wind shear, as
 370 does the uncertainty. However, it is possible and plausible that all surface precipitation
 371 originates from the mixed-phase pathway; analysis of the timing and location of surface
 372 precipitation and rain evaporation show very strong associations with the timing and lo-
 373 cation of melting and much lower correlations with autoconversion and accretion pro-
 374 cesses.

380 **4 Analysis of sensitivity in the riming rate**

381 Riming appears to be the main source of mass for hydrometeors that subsequently
 382 reach the ground. It is shown in the previous section that riming contributes more than
 383 90% to the graupel and hail mass (Figure 4b). As the mixed-phase pathway is dominant,
 384 the amount of riming therefore determines how much precipitation reaches the ground.
 385 There are several possible explanations as to why the riming rate is sensitive to CCN
 386 concentration, including: i) storm updraft size or intensity, ii) amount of available su-



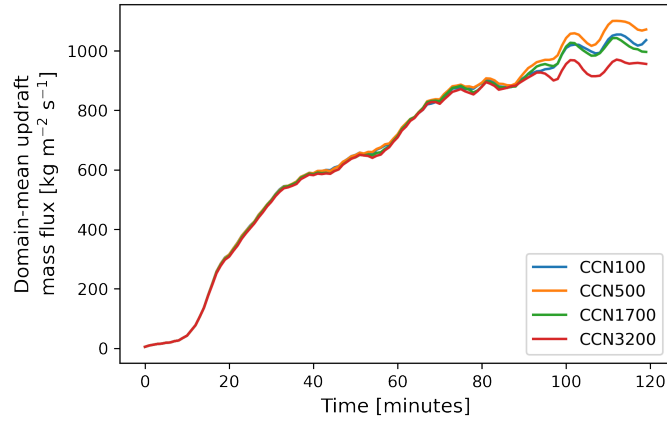
375 **Figure 5.** Summary of hydrometeor destinations, including hydrometeors still suspended at
 376 the end of the simulation period (green bars) for each simulation. Surface rain is attributed to
 377 warm and mixed-phase pathways proportional to the total sources and sinks. The error bar for
 378 warm and mixed-phase rain shows sensitivity to a factor of 5 change in assumptions about this
 379 distribution, see text for more details.

387 percooled liquid water, iii) size and concentration of cloud and rain droplets, iv) size and
 388 concentration of the graupel and hail. In this section, we attempt to attribute which of
 389 these are responsible for the changes of riming rate induced by changing the CCN con-
 390 centration in the simulations.

391 4.1 Changes to updraft characteristics

392 It is possible that the updraft characteristics changed due to increased CCN con-
 393 centrations. Feedbacks through changed latent heating from condensation or freezing,
 394 cloud edge evaporation, and additional mass of condensed hydrometeors could all po-
 395 tentially change the buoyancy and/or size of the updraft. Additionally, changes to the
 396 cold pool properties via below-cloud evaporation rates can also influence the updraft.

399 The total upward mass flux (Figure 6), histograms of updraft strength (not shown)
 400 and profiles of integrated condensation rate (not shown), each show only small changes.
 401 Total mass flux is almost unchanged throughout the first 90 minutes of the simulation.



397 **Figure 6.** Timeseries of total integrated upward mass flux from all WS18 simulations. Lines
 398 are coloured by their respective CCN concentration.

402 Thereafter, feedbacks begin to affect the updrafts leading to an approximate 10% dif-
 403 ference in the upward mass flux after 2 hours. There is no evidence of systematic effects
 404 of CCN on the simulated updrafts as would be seen if convective invigoration was oc-
 405 ccurring.

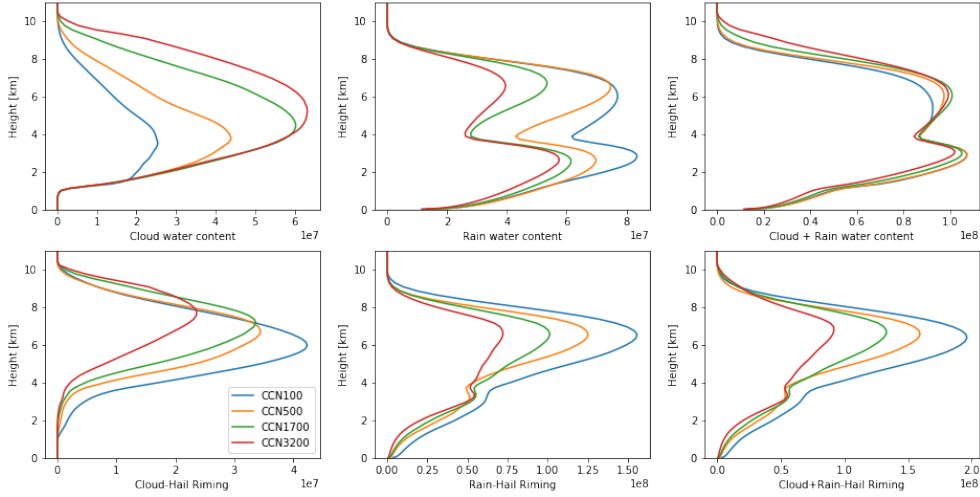
406 The changes to surface precipitation are much larger than 10% and occur before
 407 90 minutes simulation time. Therefore, we conclude that updraft changes cannot be of
 408 primary importance for surface precipitation sensitivities in these simulations.

409 **4.2 Availability of supercooled liquid water**

410 Supercooled water is a pre-requisite for the riming process. With all else being equal,
 411 riming rate increases linearly with supercooled liquid water content (SLWC; cloud plus
 412 rain water mass above the freezing level). Increased CCN results in more cloud droplets,
 413 with smaller average sizes. These smaller sized droplets collide with each other less of-
 414 ten, so the production of rain-drop-sized particles is slower. We therefore expect a dif-
 415 ference in the cloud and rain water contents inside the cloud.

416 Vertical profiles of these quantities do indeed show that cloud water mass increases
 417 with increasing CCN; however, the rain water category decreases an approximately equal
 418 amount. Despite the fact that rain droplets fall faster than cloud drops, the difference
 419 in SLWC caused by CCN concentration changes is minor (Figure 7 top row).

420 The vertical profiles of riming rates for hail collecting cloud water and rain water
 421 (Figure 7 bottom row) decrease substantially as CCN is increased. These decreases can-
 422 not be simply explained by the small changes of supercooled cloud water and rain wa-
 423 ter mass in the storm.



424 **Figure 7.** Vertical profiles of simulation-averaged domain-total cloud liquid hydrometeor
 425 contents (top row) in kg and time-averaged hail riming rates (bottom row) in kg/s. The WS32
 426 simulations are plotted. Each line represents a different CCN concentration. Plots for other wind
 427 shear simulations are qualitatively similar. The 0°C level is at 4 km altitude.

428 Previous studies [e.g. *Khain et al.*, 2011b] have hypothesised that more SLWC is
 429 present in high-CCN environments because the droplets are smaller, take longer to form
 430 large rain drop sizes and fall from the cloud and can therefore be transported higher into
 431 the cloud. However, our simulations show only a weak sensitivity of SLWC to CCN con-
 432 centration. The maximum height of SLWC does increase with increasing CCN, driven
 433 by changes in cloud water, and this does lead to an increase in riming (especially rim-
 434 ing of cloud droplets) at these heights. However, the sensitivity of riming to CCN oc-
 435 curs at lower altitudes (between 4–8 km) and is not related to increased SLWC.

436 Based on these data, we conclude that differences in SLWC cannot be the main cause
 437 of the differences in riming rates in our simulations.

438

4.3 Size-dependent riming efficiency

439

440

441

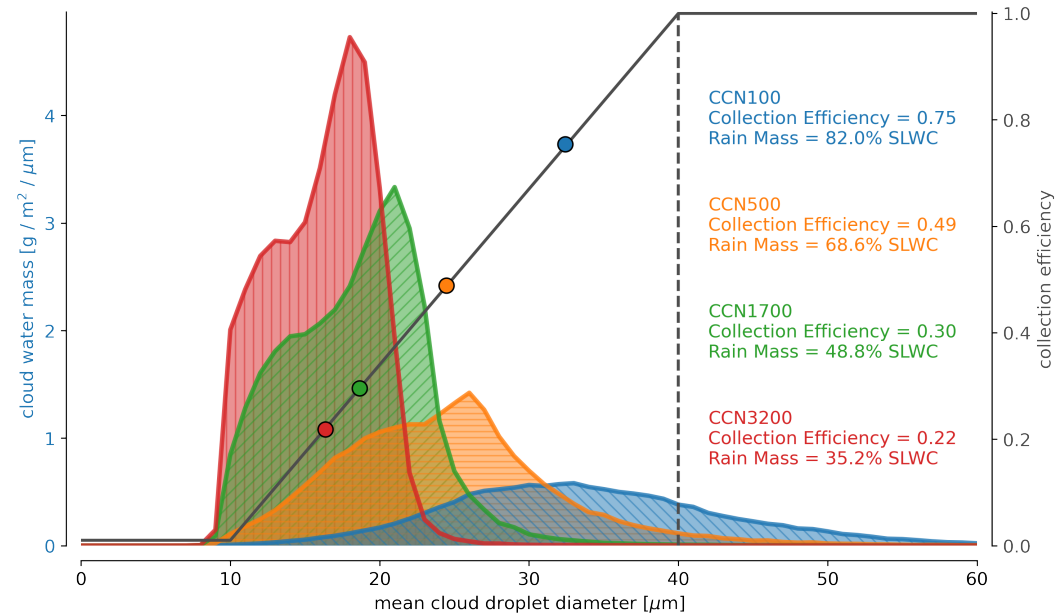
442

443

444

445

446



447

448

449

450

451

452

453

Figure 8. Parameterized riming efficiency (E_{coll} ; black line, right axis) plotted with mass-weighted histograms of the grid-box mean cloud water size distribution. Only sub-freezing grid points where riming of cloud water is occurring are included in the histograms. The histograms are plotted for the four different CCN concentrations. The mean riming efficiency is plotted along the black line with corresponding colour and quantified on the right of the plot. The percentage of supercooled water mass in the rain category is also quantified. Plots for all wind shears look similar, so only one (WS18) is shown.

454

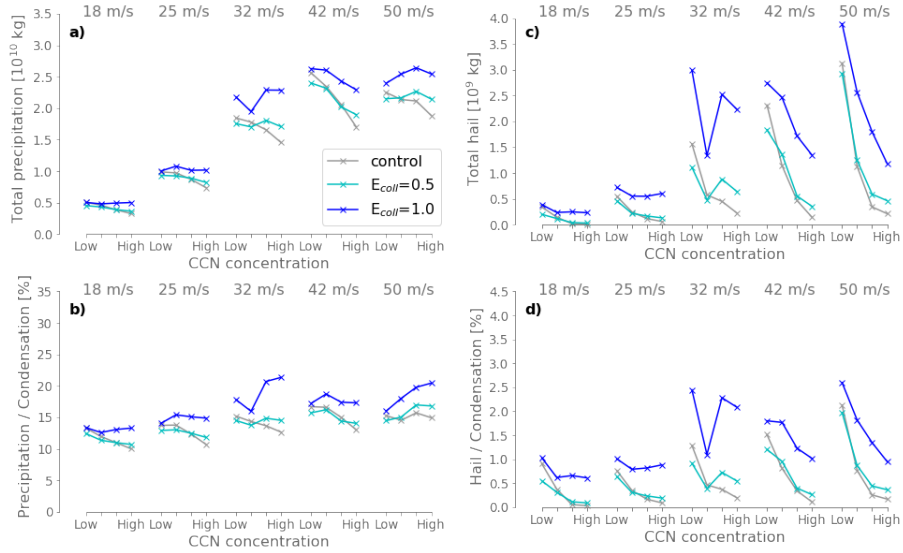
455

Cloud droplets are larger under low-CCN conditions. The riming collection efficiency for cloud droplets is parameterized as a linearly increasing function of x_c ($= q_c/n_c$; the

456 mean mass of cloud water drops within the grid box) [*Seifert and Beheng, 2006a*] and
 457 is plotted with a black line in Figure 8. Histograms of grid-box mean cloud droplet size
 458 (only at locations where riming is occurring) for simulations with different CCN concen-
 459 trations are also plotted. Equivalent plots for other wind shear values are almost iden-
 460 tical and therefore omitted. The mean riming efficiency of cloud droplets for the CCN100
 461 simulations is around 0.787, which reduces to 0.238 for the CCN3200 simulations. Rain
 462 drops are assumed to have a collection efficiency of unity and there is also increased rain
 463 water mass and less cloud water in the low-CCN simulations (Figure 7a,b) further in-
 464 creasing the sensitivity. Therefore there are two reasons to expect decreased riming rate
 465 through decreased riming efficiency as CCN is increased.

466 It is hard to theoretically estimate the effect of changing cloud drop riming efficiency
 467 on the total riming rate and hence surface precipitation. This is because the riming rate
 468 of a hail stone is related to its size. The rate of mass growth therefore increases expo-
 469 nentially over time. Hail particles with a larger initial size, or which can grow rapidly
 470 during the early stages of growth, are able to grow relatively faster later in the growth
 471 cycle. We cannot easily calculate the importance of these effects for a population of hy-
 472 drometeors in a complex 3D environment such as these simulated storms. We have there-
 473 fore performed additional simulations where the riming efficiency of cloud drops is set
 474 to constant values of 0.5 and 1.0. $E_{\text{coll}} = 0.5$ is an approximate average of riming ef-
 475 ficiency across all CCN concentrations. $E_{\text{coll}} = 1.0$ is chosen so that there was no dif-
 476 ference between the riming efficiency of rain and cloud hydrometeors.

479 The total surface precipitation and hail fall is much less sensitive to CCN concen-
 480 tration when the riming efficiency is held constant for all cloud drop sizes. Only the WS42
 481 simulations show a systematic decrease of total precipitation with $E_{\text{coll}} = 1.0$ (Figure 9a).
 482 For all simulations sets, the sensitivity of precipitation to CCN is substantially reduced
 483 in these simulations with constant E_{coll} . The sensitivity of hail fall to CCN concentra-
 484 tion is also reduced (Figure 9c). WS18 and WS25 simulations now have very little sen-
 485 sitivity. Hail in WS32 simulations responds in a non-systematic way to increased CCN.
 486 However, large sensitivities still exist for WS42 and WS50 simulation. These changes can-
 487 not be explained by changes to the storm size, as the totals when normalised by the to-
 488 tal condensation rate (Figure 9b,d) show largely similar sensitivities.



477 **Figure 9.** As Figure 1 (“control”, gray), but including simulations with E_{coll} of 0.5 (light
 478 blue) and 1.0 (dark blue).

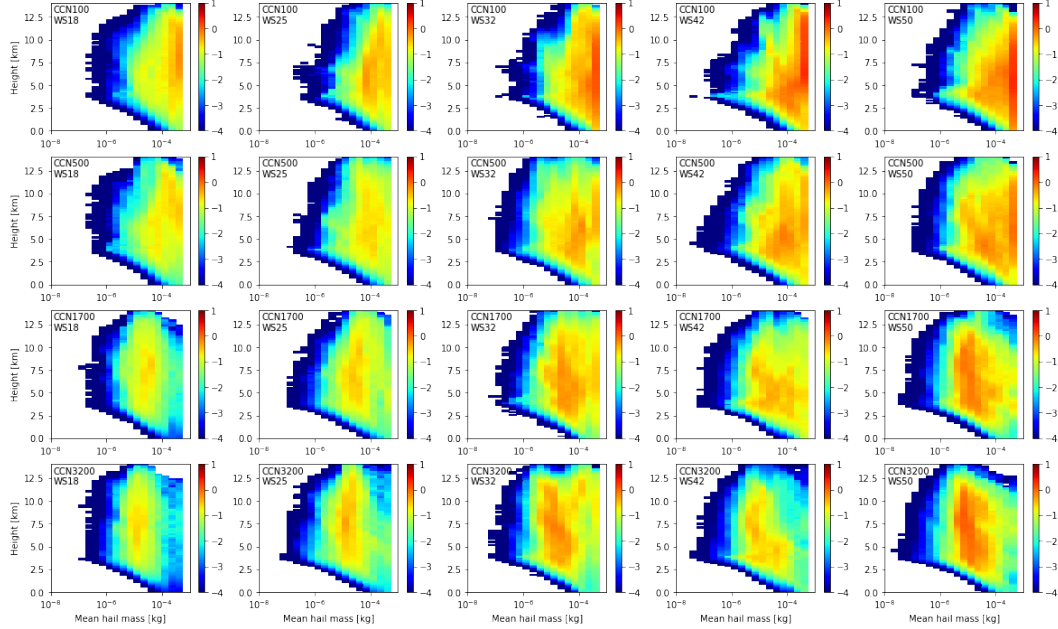
489 The much reduced sensitivity of surface precipitation and hail when riming efficiency
 490 is held constant leads us to conclude that riming efficiency is the most important fac-
 491 tor determining surface precipitation changes to CCN concentration in these simulations.
 492 Interestingly, the total precipitation and hail amounts now show some non-systematic
 493 behaviour when only CCN is increased and furthermore show different sensitivities to
 494 CCN concentration when the wind shear is changed; this behaviour is explored in the
 495 next section.

496 4.4 Size of graupel and hail particles

497 The size of the graupel and hail particles is important as it determines their po-
 498 tential to collide with supercooled water droplets. Larger graupel and hail have a larger
 499 cross-sectional area and particle fall velocity. Therefore the amount of air “swept out”
 500 by the falling hailstone within a given time increases substantially as particle size increases
 501 such that larger hail acquires more mass in a given time than small hail.

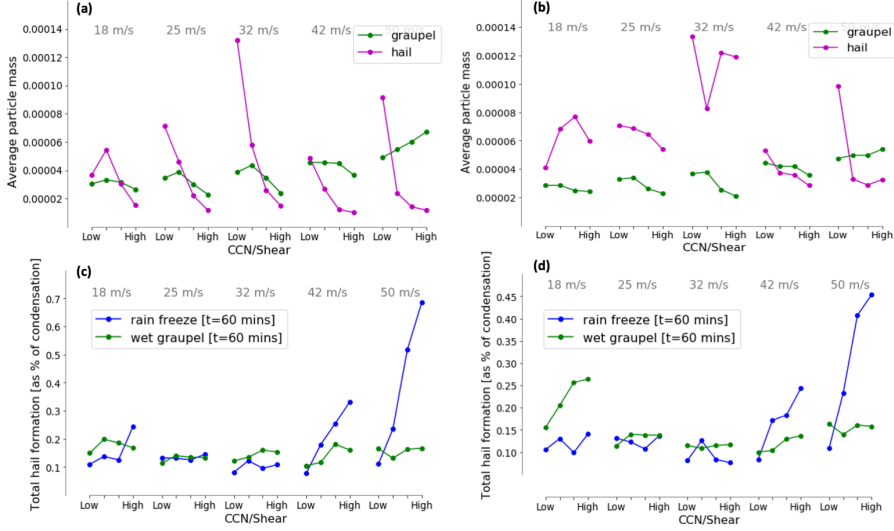
502 Furthermore, larger hail is more likely than smaller hail to reach the ground. Be-
 503 cause of their larger initial mass and faster fall velocity, large hail stones spend less time
 504 falling from the melting level to the ground. As a result, supercooled droplets which rime
 505 onto large hail are more likely to reach the surface, and to do so more quickly, than those

506 which rime onto small hail. The total surface precipitation and the storm's precipita-
 507 tion efficiency are both increased by the presence of large hail in the riming region.



508 **Figure 10.** Total hail mass as a function of height and grid-box mean hail stone mass
 509 (q_h/n_h). Each row shows simulations with the same CCN concentration (wind shear increas-
 510 ing left to right). Each column shows simulations with the same wind shear (CCN concentration
 511 increasing top to bottom). Each color pixel shows $\log_{10}(m)$, where m is total mass in kg.

512 Figure 10 shows the distribution of hail stone mass, based on the mass of the grid-
 513 box-mean hail stone size and height. Hail size reduces as the CCN concentration increases.
 514 In CCN100 simulations, the mass is concentrated towards the largest sizes. The size de-
 515 creases systematically as the CCN concentration is increased. When averaged over the
 516 whole model domain, the average particle mass for hail decreases systematically with in-
 517 creasing CCN concentration (Figure 11(a)), with only one exception (WS18+CCN500).
 518 Interestingly the mean graupel mass is not so sensitive, and for higher CCN concentra-
 519 tions the mean graupel mass is actually larger than the mean hail mass. The changed size
 520 distribution results partly from the riming efficiency decreasing with increasing CCN con-
 521 centration (see previous section). However, similar size distributions are also seen in the
 522 constant riming efficiency simulations (not shown).



523 **Figure 11.** (a) Average particle mass for all graupel and hail particles in each simulation. (b)
 524 Average particle mass for all graupel and hail particles for simulations with $E_{\text{coll}} = 1.0$. (c) Total
 525 mass (normalized by total condensation rate) of hail embryos produced by either rain freezing
 526 or conversion of graupel in the wet growth regime. Values are integrated throughout the first 60
 527 minutes of simulation time. (d) Same for simulations with $E_{\text{coll}} = 1.0$.

528 A more important factor for these differences is the size of hail embryos produced
 529 in the simulation. There are two active mechanisms that produce initial hail embryos:
 530 freezing of rain drops and conversion of graupel to hail when wet growth begins. The
 531 details of these two processes are given in section 2. The formation of (smaller) hail em-
 532 bryos by rain freezing produces equal or less mass than the formation of (larger) hail em-
 533 bryos by conversion of graupel for simulations with wind shear up to 32 m/s (Figure 11(c)).
 534 For WS42 and WS50 simulations, the rain freezing process produces more mass and is
 535 very sensitive to the CCN concentration: increased CCN concentration leads to increased
 536 rain freezing. This is equally true for simulations where $E_{\text{coll}} = 1.0$ (Figure 11(d)).

537 There is a strong link between the mean size of hail in the simulations and the for-
 538 mation mechanism. Large hail sizes are seen in simulations where wet growth of grau-
 539 pel is the primary mechanism. Smaller sizes occur when rain freezing is the primary mech-
 540 anism. Smaller hail is more likely to melt fully when falling, therefore the total hail fall
 541 is substantially reduced in simulations where only small hail is produced (the high-CCN
 542 simulations). A negative correlation is found between total surface hail (Figure 1(b)) and

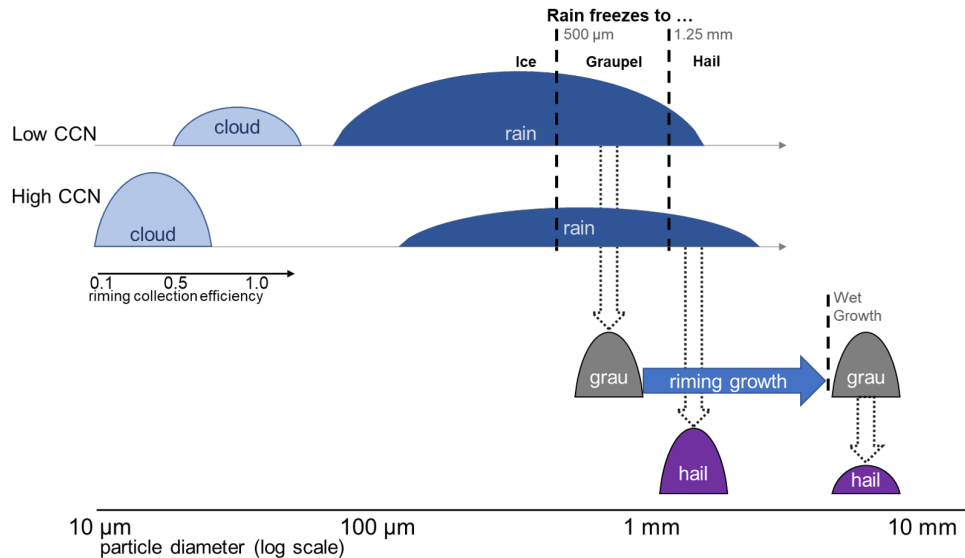
543 the rate of hail formation by rain freezing (Figure 11(c)). The correlation is especially
 544 clear when the collection efficiency is set to unity (Figures 9(b) and 11(d)) and most ob-
 545 vious when more hail is formed from rain freezing than by graupel undergoing wet growth.

546 **4.5 Summary on hail sensitivity to CCN**

547 Increased riming rates for graupel and hail are observed with decreasing CCN con-
 548 centration, but this does not result from changes in updraft characteristics or changed
 549 supercooled liquid water mass in the cloud. Rather, the characteristics of the cloud and
 550 rain droplets themselves are important, and in particular their size, which impacts the
 551 possible microphysical pathways of hail formation (Figure 12). Lower CCN concentra-
 552 tions therefore produce more hail fall at the surface for the following reasons:

- 553 1. Lower CCN concentration means fewer but larger cloud drops. Larger cloud drops
 554 have a higher riming efficiency than small cloud drops.
- 555 2. Larger cloud drops are more likely to become rain drops. Rain drops have a higher
 556 riming efficiency than cloud drops.
- 557 3. Lower CCN concentrations result in less rain freezing on average, although this
 558 is sometimes a non-systematic signal. Hail embryos formed through conversion of
 559 graupel in the wet growth regime produce larger embryos than when formed by
 560 freezing of rain drops. Larger hail embryos grow to become larger hail stones which
 561 are more likely to reach the surface.

562 The change of cloud drop riming efficiency with size is the primary reason for changed
 563 surface precipitation totals in these simulations. When the riming efficiency does not change
 564 with particle size, the CCN sensitivity of the surface precipitation rate is largely removed.
 565 However, the sensitivity of hail fall to CCN still remains for higher wind shear environ-
 566 ments (≥ 32 m/s). These (sometimes non-systematic) changes of hail fall with increas-
 567 ing CCN concentration are explained by changes to hail embryo sizes. Two different mech-
 568 anisms are responsible for producing hail embryos in the simulation: rain freezing (smaller
 569 embryos) and conversion of graupel (larger embryos). Simulations where rain freezing
 570 is the most active (typically high wind shear and high CCN concentrations) produce the
 571 least surface hail.



572 **Figure 12.** Schematic plot illustrating the two different hail embryo formation pathways.
 573 Each semicircle represents an approximate size distribution. Changes of particle class are marked
 574 by dotted arrows. Hail formed by rain freezing is much smaller than hail created (in the model)
 575 when graupel reaches the wet growth regime. The relative amount of these two hail formation
 576 pathways depends on the rain drop size distribution, which in turn is affected by the CCN con-
 577 centration.

578 5 Discussion

579 We found that most surface precipitation (whether hail or rain) is formed through
 580 the mixed-phase pathway. Riming is the most important process contributing mass in
 581 the mixed-phase pathway and we found that the cloud and rain drop size distributions
 582 play an important role; larger drop sizes result in faster growth by riming. The avail-
 583 ability of large supercooled droplets (whether rain drops or large cloud droplets with high
 584 collection efficiency) was important for the formation of large rimed hydrometeors, and
 585 it is these large rimed hydrometeors that are responsible for at least two thirds of the
 586 surface precipitation. The sensitivity to drop sizes highlights the importance of CCN con-
 587 centration, even though the contribution of the warm rain pathway to surface precip-
 588 itation was negligible.

589 Our results may help to explain the large sensitivity of precipitation in simulations
 590 of deep convection to chosen microphysical properties found in previous studies. E. g.,
 591 *White et al.* [2017] found that swapping the autoconversion parameterization between

592 two different microphysics parameterizations schemes affected the simulated precipita-
593 tion more than changing the CCN concentration did. Therefore, the results of *White et al.*
594 [2017] may be understood through this mechanism, as the increased availability of large
595 supercooled (rain) hydrometeors should produce additional precipitation. Our analysis
596 of the microphysical pathways gives a new framework for understanding how changes to
597 the warm-rain physics have large impacts on the evolution and precipitation from con-
598 vective storms. Changes made via changing CCN concentration (as in this study), chang-
599 ing the autoconversion parameterization [as in *White et al.*, 2017] or changing the pa-
600 rameters of the cloud droplet size distribution (such as N_0 , μ , ν) [e.g., *Barthlott et al.*,
601 2022] potentially lead to similar physical sensitivities and could be understood consis-
602 tently. More research comparing these sensitivities is needed.

603 The sensitivity of surface precipitation and hail to supercooled hydrometeor size
604 is plausible in reality. Our study is limited to analysis of simulated convective cells; how-
605 ever, evidence from radar observations also suggests that large raindrops are present when
606 hail formation occurs. A so-called “ZDR column”, a vertically coherent region of increased
607 differential reflectivity (ZDR) values, is often detected in dual-polarimetric observations
608 of convective cells which are producing hail, and the ZDR column depth has been shown
609 to be a good predictor of large hail formation [*Kumjian et al.*, 2014; *Ilotoviz et al.*, 2018;
610 *Kuster et al.*, 2019]. Large ZDR values are interpreted as being a signal of large oblate
611 liquid hydrometeors several mm in diameter (such as large rain drops), and have been
612 observed to extend 3 km above the melting level. The presence of the ZDR column can
613 be used for nowcasting hail in the next 10-15 minutes [*Kumjian et al.*, 2014]. It is there-
614 fore plausible that the sensitivities and mechanisms relating to riming efficiency discussed
615 in this article apply not only to idealised simulations but also to real convective cells.
616 Nevertheless, more realistic simulations combined with observational evidence are needed
617 to confirm this.

618 The second important sensitivity, to the process producing hail embryos, is more
619 difficult to link to reality, although early studies have attempted to identify hail embryos
620 and their properties in photographs of hailstone sections [e. g., *Knight and Knight*, 1970].
621 Reality does not have separate categories for graupel and hail. Therefore whether the
622 diameter of a frozen raindrop exceeds a threshold size does not determine its classifica-
623 tion or affect its chance of becoming a large hail stone later. Larger sized frozen drops
624 do grow faster, but their characteristics (such as density and fall velocity) are determined

625 by the current size not by the initial size at formation. In the model representation, this
626 can only change if a graupel stone enters the wet growth regime and gets reclassified as
627 hail. It is therefore likely that the surface precipitation and potentially the CCN sen-
628 sitivity depends on the threshold sizes in the rain freezing parameterization. A similar
629 analysis using the Predicted Particle Properties [P3 *Morrison and Milbrandt, 2015*] mi-
630 crophysics scheme, where particle density can evolve with time, or using particle trajec-
631 tory calculations [*Kumjian and Lombardo, 2020*] would both be helpful to check the ro-
632 bustness of these results.

633 The relatively large sensitivity to CCN concentration could also be interpreted as
634 a consequence of “beneficial” competition between the many, small hail embryos formed
635 by freezing of rain drops. Although the partially-arbitrary classification of frozen rain
636 drops as graupel or hail is potentially leading to an artificially strong effect, the impor-
637 tance of beneficial competition among growing hail has been theorised in the context of
638 hail suppression [e. g., *Atlas, 1977*].

639 The accuracy of the riming calculations in the model is of importance because the
640 riming process was the most important for producing surface precipitation in these sim-
641 ulations. The Seifert and Beheng scheme represents riming quite accurately. It use a col-
642 lision kernel, based on the full particle size distributions of both hydrometeor species in-
643 volved in each calculated collision type. The only simplification relates to the riming ef-
644 ficiency, which is a) represented by a linear function of liquid droplet size between two
645 thresholds and b) uses the grid-box mean particle size rather than integrating over the
646 full size distribution. A representation such as that in the “bin-emulating” approach of
647 *Saleeby and Cotton [2008]* would be more accurate and the benefit of such representa-
648 tion in ICON should be quantified in a future study.

649 **6 Conclusions**

650 Simulations with the ICON model have been used to identify the chain of processes
651 producing precipitation, referred to here as “microphysical pathways”, in idealised thun-
652 derstorms. The relative importance of each pathway and their sensitivity to CCN con-
653 centration and wind shear have been quantified.

654 In all simulations, 86–100% of surface precipitation resulted from the melting of
655 frozen hydrometeors. These hydrometeors followed the mixed-phase pathway, where the

656 main source of mass came from riming. Almost no surface rain was produced via the warm-
657 rain pathway (through collision and coalescence parameterized as autoconversion and
658 accretion). No precipitation occurred as the result of melting of ice or snow (the ice-phase
659 pathway). A substantial fraction ($\geq 50\%$) of all condensed mass remained in the atmo-
660 sphere at the end of the simulations (the non-precipitating pathway), mostly as small
661 ice and small graupel, both at high-altitudes.

662 The mixed-phase pathway remains dominant pathway for all CCN and wind shear
663 setups. However, the overall efficiency of converting condensed mass to surface precip-
664 itation is decreased by increased CCN concentration. Increasing wind shear led to in-
665 creased surface rain and hail in almost all situations but it was distributed over a larger
666 area meaning that the local maxima remained similar.

667 Further breaking down the mixed-phase pathway, there are two important factors
668 that determine the final precipitation and hail totals: riming efficiency and hail embryo
669 size. The riming efficiency, determined by the size of the liquid droplets in each collision,
670 determines how much precipitation mass reaches the surface. Increased riming efficien-
671 cies allow mass to be transferred faster to graupel and hail, leading to larger hydrom-
672 eteors and increased precipitation totals. Lower CCN concentrations result in larger drop
673 sizes and therefore more precipitation. Hail embryo size is determined by how the em-
674 bryo is formed. Larger hail embryos (as formed when graupel is reclassified as hail in the
675 model) acquire mass more quickly than smaller embryos (mostly formed through freez-
676 ing of rain drops). Therefore simulated storms with substantial rain freezing contain many
677 small hail embryos which grow and fall more slowly than larger hail, allowing them to
678 melt fully before reaching the surface.

679 The riming process, part of the mixed-phase pathway where falling frozen hydrom-
680 eteors collide with and collect supercooled liquid droplets, was the most important pro-
681 cess for producing hydrometeors which contribute to surface precipitation. Although the
682 warm-rain pathway did not contribute to surface precipitation, the warm-phase prop-
683 erties of the cloud (number concentration, 3D distribution and size of cloud and rain drops)
684 played an important role in the precipitation process - due to the importance of riming.
685 The properties of the liquid drops determine the efficiency at which they are collected
686 by falling frozen hydrometeors, with larger drops more likely to be collected. Therefore,

687 the presence of rain and large cloud drops ($\geq 40 \mu\text{m}$) in regions where frozen hydrom-
688 eteors fall is critical for the amount of surface precipitation produced.

689 Increasing the CCN concentration produced smaller and more numerous cloud droplets
690 and also affected the size and concentration of rain drops within the cloud, and there-
691 fore surface precipitation. The smaller cloud drops slow precipitation production via the
692 mixed-phase pathway in two ways: 1) the smaller cloud drops are collected less efficiently
693 by falling frozen hydrometeors and 2) the cloud drops grow to the size of rain drops more
694 slowly, maintaining their low collection efficiency for longer. Increased CCN concentra-
695 tion therefore leads to an increased mass of hydrometeor mass suspended in the atmo-
696 sphere and smaller precipitation particles, increasing the chance of melting and/or evap-
697 oration before reaching the surface and therefore reducing the surface precipitation and
698 hail totals.

699 Removing the size dependence of the riming efficiency largely removed the sensi-
700 tivity of surface precipitation to CCN. However, the surface hail totals still showed sensi-
701 tivity to CCN concentration in some setups, especially those with high wind shear ($\geq 32 \text{ m/s}$).
702 The remaining sensitivity related to hail embryo size. More hail embryos were formed
703 at high CCN concentrations but they were smaller; the total hail embryo mass was al-
704 most constant for all CCN concentrations. The hail stones then grew more slowly, reached
705 smaller maximum sizes and were more likely to melt fully before reaching the surface.
706 As illustrated in Figure 12, the largest hail embryos were produced when graupel became
707 hail as it entered the wet growth regime. Rain freezing produced smaller hail embryos
708 on average. Simulations with large amounts of hail produced by rain freezing (e.g. high
709 CCN concentration) therefore had the smallest hail stones and the least surface hail, even
710 when the riming efficiency did not depend on liquid drop size.

711 Although the results presented in this paper come only from idealised model sim-
712 ulations, the formation of hail in the presence of large supercooled hydrometeors appears
713 consistent with observations of ZDR columns in radar observations. These columns of
714 positive ZDR are thought to indicate regions of large oblate liquid hydrometeors and are
715 indicative of convective cells likely to produce hail. On the other hand, the model sen-
716 sitivity of surface precipitation and hail to hail embryo formation mechanism is not cur-
717 rently supported by any observational evidence. The mechanism may be dependent on
718 certain size thresholds defined in the model parameterizations. Further model and ob-

719 servational studies are needed to determine the importance of hail embryo size and their
720 associated formation mechanisms.

721 As detailed in the introduction, there is currently no consensus in the literature about
722 the sign of the sensitivity of surface precipitation or hail to changed CCN concentrations.
723 Therefore, our results agree with some of the existing literature and disagree with other
724 studies. However, the method presented here to understand the relative sensitivities of
725 different microphysical pathways can be used to determine whether the sensitivities in
726 ICON are consistent for other environmental conditions and can be applied in other mod-
727 els/microphysical parameterizations too. Application of this microphysical pathway anal-
728 ysis to other simulation datasets with diverse responses of precipitation to CCN pertur-
729 bations may help explain the origin of these differences.

730 **7 Open Research**

731 Post-processed data from the model simulations will be made available in the open
732 access repository KITopen once the paper has been accepted for publication. The ICON
733 model source code is license protected.

734 **Acknowledgments**

735 The research leading to these results was partly performed within subproject B1 of the
736 Transregional Collaborative Research Center SFB / TRR 165 “Waves to Weather” funded
737 by the German Research Foundation (“Deutsche Forschungsgemeinschaft”, DFG). Ad-
738 ditional work was performed under the subproject “Evaluating and Improving Convection-
739 Permitting Simulations of the Life Cycle of Convective Storms using Polarimetric Radar
740 Data” under the programme SPP-2115 “PROM”. CH acknowledges funding from the
741 European Research Council (ERC) under the European Union’s Horizon 2020 research
742 and innovation programme under grant agreement No 714062 (ERC Starting Grant “C2Phase”).
743 This work was performed on the computational resource ForHLR II funded by the Min-
744 istry of Science, Research and the Arts Baden-Württemberg and DFG.

745 **References**

746 Atlas, D. (1977), The paradox of hail suppression, *Science*, 195(4274), 139–145,
747 doi:10.1126/science.195.4274.139.

- 748 Barrett, A. I., C. Wellmann, A. Seifert, C. Hoose, B. Vogel, and M. Kunz (2019),
749 One Step at a Time: How Model Time Step Significantly Affects Convection-
750 Permitting Simulations, *Journal of Advances in Modeling Earth Systems*, doi:
751 10.1029/2018MS001418.
- 752 Barthlott, C., A. Zarbo, T. Matsunobu, and C. Keil (2022), Importance of aerosols
753 and shape of the cloud droplet size distribution for convective clouds and precip-
754 itation, *Atmospheric Chemistry and Physics*, *22*(3), 2153–2172, doi:10.5194/acp-
755 22-2153-2022.
- 756 Bigg, E. (1953), The formation of atmospheric ice crystals by the freezing of
757 droplets, *Quarterly Journal of the Royal Meteorological Society*, *79*(342), 510–
758 519.
- 759 Blahak, U. (2008), Towards a better representation of high density ice particles in
760 a state-of-the-art two-moment bulk microphysical scheme, *Proc. 15th Int. Conf.*
761 *Clouds and Precip., Cancun, Mexico*.
- 762 Carrió, G. G., W. R. Cotton, and A. Loftus (2014), On the response of hailstorms to
763 enhanced ccn concentrations, *Atmospheric research*, *143*, 342–350.
- 764 Chen, Q., Y. Yin, H. Jiang, Z. Chu, L. Xue, R. Shi, X. Zhang, and J. Chen (2019),
765 The roles of mineral dust as cloud condensation nuclei and ice nuclei during the
766 evolution of a hail storm, *Journal of Geophysical Research: Atmospheres*, *124*(24),
767 14,262–14,284.
- 768 Ilotoviz, E., A. Khain, A. V. Ryzhkov, and J. C. Snyder (2018), Relationship be-
769 tween aerosols, hail microphysics, and zdr columns, *Journal of the Atmospheric*
770 *Sciences*, *75*(6), 1755 – 1781, doi:10.1175/JAS-D-17-0127.1.
- 771 Khain, A., D. Rosenfeld, A. Pokrovsky, U. Blahak, and A. Ryzhkov (2011a), The
772 role of CCN in precipitation and hail in a mid-latitude storm as seen in simula-
773 tions using a spectral (bin) microphysics model in a 2D dynamic frame, *Atmo-*
774 *spheric Research*, doi:10.1016/j.atmosres.2010.09.015.
- 775 Khain, A., D. Rosenfeld, A. Pokrovsky, U. Blahak, and A. Ryzhkov (2011b), The
776 role of ccn in precipitation and hail in a mid-latitude storm as seen in simulations
777 using a spectral (bin) microphysics model in a 2d dynamic frame, *Atmospheric*
778 *Research*, *99*(1), 129–146.
- 779 Khain, A. P., N. BenMoshe, and A. Pokrovsky (2008), Factors Determining the
780 Impact of Aerosols on Surface Precipitation from Clouds: An Attempt at Classifi-

- 781 cation, *Journal of the Atmospheric Sciences*, doi:10.1175/2007JAS2515.1.
- 782 Khain, A. P., K. D. Beheng, A. Heymsfield, A. Korolev, S. O. Krichak, Z. Levin,
783 M. Pinsky, V. Phillips, T. Prabhakaran, A. Teller, S. C. Van Den Heever,
784 and J. I. Yano (2015), Representation of microphysical processes in cloud-
785 resolving models: Spectral (bin) microphysics versus bulk parameterization,
786 doi:10.1002/2014RG000468.
- 787 Knight, C. A., and N. C. Knight (1970), Hailstone embryos, *Journal of Atmospheric*
788 *Sciences*, 27(4), 659 – 666, doi:10.1175/1520-0469(1970)027<0659:HE>2.0.CO;2.
- 789 Kumjian, M. R., and K. Lombardo (2020), A hail growth trajectory model for ex-
790 ploring the environmental controls on hail size: Model physics and idealized tests,
791 *Journal of the Atmospheric Sciences*, 77(8), 2765–2791.
- 792 Kumjian, M. R., A. P. Khain, N. Benmoshe, E. Ilotoviz, A. V. Ryzhkov, and
793 V. T. J. Phillips (2014), The anatomy and physics of zdr columns: Investigating a
794 polarimetric radar signature with a spectral bin microphysical model, *Journal of*
795 *Applied Meteorology and Climatology*, 53(7), 1820 – 1843, doi:10.1175/JAMC-D-
796 13-0354.1.
- 797 Kuster, C. M., J. C. Snyder, T. J. Schuur, T. T. Lindley, P. L. Heinselman, J. C.
798 Furtado, J. W. Brogden, and R. Toomey (2019), Rapid-update radar observations
799 of zdr column depth and its use in the warning decision process, *Weather and*
800 *Forecasting*, 34(4), 1173 – 1188, doi:10.1175/WAF-D-19-0024.1.
- 801 Lebo, Z. J., H. Morrison, and J. H. Seinfeld (2012), Are simulated aerosol-induced
802 effects on deep convective clouds strongly dependent on saturation adjustment?,
803 *Atmospheric Chemistry and Physics*, doi:10.5194/acp-12-9941-2012.
- 804 Loftus, A., and W. Cotton (2014), Examination of ccn impacts on hail in a sim-
805 ulated supercell storm with triple-moment hail bulk microphysics, *Atmospheric*
806 *research*, 147, 183–204.
- 807 Marion, G. R., and R. J. Trapp (2019), The dynamical coupling of convec-
808 tive updrafts, downdrafts, and cold pools in simulated supercell thunder-
809 storms, *Journal of Geophysical Research: Atmospheres*, 124(2), 664–683, doi:
810 <https://doi.org/10.1029/2018JD029055>.
- 811 Morrison, H. (2012), On the robustness of aerosol effects on an idealized supercell
812 storm simulated with a cloud system-resolving model, *Atmospheric Chemistry and*
813 *Physics*, 12(16), 7689–7705.

- 814 Morrison, H., and J. A. Milbrandt (2015), Parameterization of cloud microphysics
815 based on the prediction of bulk ice particle properties. part i: Scheme description
816 and idealized tests, *Journal of Atmospheric Sciences*, *72*(1), 287–311.
- 817 Noppel, H., U. Blahak, A. Seifert, and K. D. Beheng (2010), Simulations
818 of a hailstorm and the impact of CCN using an advanced two-moment
819 cloud microphysical scheme, *Atmospheric Research*, *96*(2-3), 286–301, doi:
820 10.1016/j.atmosres.2009.09.008.
- 821 Phillips, V. T. J., P. J. DeMott, and C. Andronache (2008), An empirical pa-
822 rameterization of heterogeneous ice nucleation for multiple chemical species
823 of aerosol, *Journal of the Atmospheric Sciences*, *65*(9), 2757 – 2783, doi:
824 10.1175/2007JAS2546.1.
- 825 Saleeby, S. M., and W. R. Cotton (2008), A binned approach to cloud-droplet riming
826 implemented in a bulk microphysics model, *Journal of Applied Meteorology and
827 Climatology*, *47*(2), 694–703.
- 828 Segal, Y., and A. Khain (2006), Dependence of droplet concentration on aerosol
829 conditions in different cloud types: Application to droplet concentration param-
830 eterization of aerosol conditions, *Journal of Geophysical Research Atmospheres*,
831 *111*(15), doi:10.1029/2005JD006561.
- 832 Seifert, A., and K. D. Beheng (2001), A double-moment parameterization for sim-
833 ulating autoconversion, accretion and selfcollection, *Atmospheric Research*, doi:
834 10.1016/S0169-8095(01)00126-0.
- 835 Seifert, A., and K. D. Beheng (2006a), A two-moment cloud microphysics param-
836 eterization for mixed-phase clouds. Part 1: Model description, *Meteorology and
837 Atmospheric Physics*, doi:10.1007/s00703-005-0112-4.
- 838 Seifert, A., and K. D. Beheng (2006b), A two-moment cloud microphysics param-
839 eterization for mixed-phase clouds. Part 2: Maritime vs. continental deep convec-
840 tive storms, *Meteorology and Atmospheric Physics*, doi:10.1007/s00703-005-0113-3.
- 841 Stevens, B., and G. Feingold (2009), Untangling aerosol effects on clouds and precip-
842 itation in a buffered system, *Nature*, *461*, 607613.
- 843 Tao, W.-K., J.-P. Chen, Z. Li, C. Wang, and C. Zhang (2012), Impact of aerosols
844 on convective clouds and precipitation, *Reviews of Geophysics*, *50*(2), doi:
845 <https://doi.org/10.1029/2011RG000369>.

- 846 Warren, R. A., H. Richter, H. A. Ramsay, S. T. Siems, and M. J. Manton (2017),
847 Impact of variations in upper-level shear on simulated supercells, *Monthly*
848 *Weather Review*, *145*(7), 2659–2681.
- 849 Weisman, M. L., and J. B. Klemp (1982), The Dependence of Numerically Simu-
850 lated Convective Storms on Vertical Wind Shear and Buoyancy, *Monthly Weather*
851 *Review*, doi:10.1175/1520-0493(1982)110<0504:TDONSC>2.0.CO;2.
- 852 Wellmann, C., A. Barrett, J. Johnson, M. Kunz, B. Vogel, K. Carslaw, and C. Hoose
853 (2018), Using emulators to understand the sensitivity of deep convective clouds
854 and hail to environmental conditions, *Journal of Advances in Modeling Earth*
855 *Systems*, *10*(12), 3103–3122.
- 856 White, B., E. Gryspeerd, P. Stier, H. Morrison, G. Thompson, and Z. Kipling
857 (2017), Uncertainty from the choice of microphysics scheme in convection-
858 permitting models significantly exceeds aerosol effects, *Atmospheric Chemistry*
859 *and Physics*, doi:10.5194/acp-17-12145-2017.